

X point effects on the ideal MHD modes in tokamaks in the description of dual-poloidal-region safety factor

Linjin Zheng,* M. T. Kotschenreuther, F. L. Waelbroeck, and M. E. Austin
Institute for Fusion Studies, University of Texas at Austin, Austin, TX 78712

(Dated: November 4, 2024)

The flux coordinates with dual-region safety factor (q) in the poloidal direction are developed in this work. The X-point effects on the ideal MHD modes in tokamaks are then analyzed using this coordinate system. Since the X-point effects mainly affect the edge region, the modes localized at the tokamak edge are particularly examined. Two types of modes are studied. The first is related to the conventional peeling or peeling-ballooning modes. The mode existence aligned with the local magnetic field in the poloidally core region as observed experimentally is confirmed. The X points are shown to contribute to a stabilizing effect for the conventionally treated modes with the surface-averaged q and with the tokamak edge portion truncated. The other is the axisymmetric modes localized in the vicinity of X points, which can affect the cross-field-line transport near the X points. The existence of axisymmetric modes points to the possibility of applying a toroidally axisymmetric resonant magnetic perturbation (RMP) in the X-point area for mitigating the edge localized modes, which can be an alternative to the current RMP design. The dual q description also has important implications for the existing non-axisymmetric RMP concept. It helps to understand why the RMP suppression of edge localized modes is difficult to achieve in the double-null tokamak configurations and points to the possibility of further improving the current RMP concept by considering the alignment to the local q .

PACS numbers: 52.53.Py, 52.55.Fa, 52.55.Hc

I. INTRODUCTION

Nowadays, the high mode (H mode) confinement has become the standard scheme for conventional tokamaks with positive triangularity.¹ However, the H mode confinement is often tied with the so-called edge localized modes (ELMs), that can discharge the pedestal heat to divertors.¹ Such a discharge may severely damage the divertors. Theoretically, the peeling-ballooning modes have been accepted as the interpretation of ELMs,² Nevertheless, the separatrix effects (or X-point effects) on the plasma edge stability remain an active research subject. An important progress about the separatrix effects on the ballooning modes has been made in Ref. 3. It has been employed to explain the physics picture of tokamak H-mode confinement.⁴ There are also other investigations based on the model equilibria, for example in Refs. 5 and 6. References 7 and 8 also reported the stabilization of a toroidal plasma's separatrix in magnetohydrodynamic (MHD) description. Numerically, the GATO and KINX codes are also developed to compute the X-point effects with the finite element method.^{9,10} Both GATO and KINX have been routinely used to study the MHD stability of the equilibria with X points, for example in Refs. 11 and 12. Different from the Fourier-decomposition-based codes, the finite-element-based codes provide the possibility to address the issue of high local safety factor q (i.e., small field line pitch) in the vicinity of X points. In

this work, we introduce an alternative approach based on the dual q coordinates to treat this problem. Besides, as shown in the recent paper Ref. 13, the plasma boundary near the X point can only be of the hyperbola type or in the X shape with the plasma segment in a right angle (i.e., 90 degrees). This shows that the equilibria used by some early studies of X-point effects need to be modified. As will be seen, our current theory, however, works with the Solovév equilibrium¹⁴ with the tiny thin edge layer truncated. As will be seen, the main difference from the previous works lies in that the dual q coordinates are used in the current work.

In fact, in a tokamak, the poloidal magnetic field vanishes only at the X point. If one introduces the local safety factor, it tends to infinity only at the X points, while remaining finite elsewhere. It is the surface average in the definition of q in the conventional flux coordinates that makes the safety factor tend to infinity everywhere on a surface as approaching the plasma edge. This can be seen later on in the main text in the flux coordinate representation of magnetic field in Eq. (1) and the definition of q in Eq. (2). Using the surface-averaged safety factor can be misleading in interpreting the relevant physics at the plasma edge. Experimentally, the MAST experimental observation as shown in Fig. 1 indicates that the perturbation filaments actually are aligned with the local magnetic field line, i.e., following the local q .^{15,16} It, therefore, does not fit the surface-averaged q description. In the surface-averaged q description, the poloidal and toroidal wave numbers, k_θ and k_ψ , for the modes aligned with the local q in the poloidally core region would become infinite in the vicinity of X points.^{4,5} This does not appear in Fig. 1. Theoretically, in the

*Corresponding author: Linjin Zheng,
email: lzheng@austin.utexas.edu

surface-averaged q description, the Alfvén resonance condition $m - nq = 0$ requires that for a finite toroidal mode number n , the poloidal mode number m has to be infinite due to $q \rightarrow \infty$. This implies that the perpendicular wavelength turns to vanish. This certainly does not reflect experimental observations and is also unacceptable physically, especially for MHD description. The perpendicular wavelength cannot be shorter than the Larmor radius for the MHD formalism to be relevant. Furthermore, if the surface-averaged q is used, the extremely large magnetic shear appears everywhere on the last few closed flux surfaces, which again oversimplifies the equilibrium description. The magnetic shear only becomes extremely large in the vicinity of X point. There are consequences for this oversimplified description. For example, since the apparent mass effect is proportional to the safety factor square, the surface-averaged q leads the mass of parallel motion to become extremely large everywhere on the last few closed flux surfaces, and so are the finite Larmor radius effects. All of these show that one should give up the single surface-averaged q description at the plasma edge.

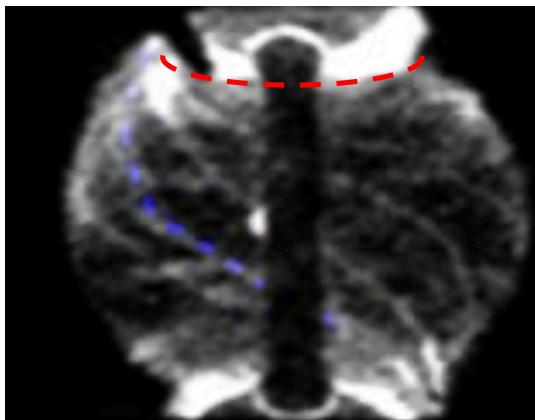


FIG. 1: The peeling ballooning filaments observed in the MAST experiment, The blue dashed and newly introduced red dashed curves mark two typical field line pitches in regions Θ_{core} and Θ_X respectively. Reprinted with permission from A. Kirk, et al., *Phys. Rev. Lett.* **96**, 185001 (2006),¹⁵ Copyright (2006) by the American Physical Society.

Let us discuss further the experimental observation. From physics consideration, other than that the MHD perturbation follows the local field line as pointed out in Ref. 15, one would not expect otherwise unless the non-ideal MHD effects play a role. Noting that the actual q is of dual regions in the poloidal direction, one would not expect the confinement of plasma to behave differently in the experiments. One may argue that the filament structure shown in Fig. 1 looks like the usual ballooning mode feature with $k_{\parallel} \ll k_{\perp}$, where k_{\parallel} and k_{\perp} are respectively the parallel and perpendicular wave numbers. Actually, it is not. The subtle physics picture of flux-tube-like modes, like the ballooning or interchange type of modes,

needs to be considered. For the flux-tube-type modes, one needs to examine the field line bundle inside the flux tube, instead of a single field line pitch. In doing so, one sees that the bundle shrinks sharply from the poloidally core region to the X point or expands dramatically from the X point to the poloidally core region. The flux tube modes tied to the field line bundle with finite width in the perpendicular region in the poloidally core region (blue dashed curve in Fig. 1) are fundamentally different from the flux tube modes tied to the field line bundle with finite width in the perpendicular region in the vicinity of X points (red dashed curve in Fig. 1). This indicates there can be two primary modes: one aligns with the local field line pitch in the poloidally core region and the other follows the field lines in the vicinity of X point. This picture goes beyond oversimplified considerations based on a single field line pitch without taking into account the field-line-bundle shrinkage or expansion. This shows that the dual-poloidal-region q description is more appropriate in considering this dual mode feature.

Let us also discuss further the numerical treatment of X point effects. Leaving aside the existence issue of the X point equilibrium as pointed out in Ref. 13, the single surface-averaged q description results in an infinite number of rational surfaces at plasma edge in the radial direction and the requirement of infinite poloidal Fourier harmonics (or highly dense poloidal grids) to describe it. None of the existing MHD codes based on the surface-averaged q to represent the magnetic field can handle this situation. Even if it did, the distance between the rational surfaces or the perpendicular wavelength of high m modes would be well below the Larmor radius. This makes the MHD description inapplicable in the vicinity of X point. To explain this, we introduce the schematic plot of magnetic field line pattern in Fig. 2. In the inner and outer boards of plasma torus (Θ_{core}) the field lines have a finite pitch. However, in the vicinity of X point, the pitch tends to zero and the distance from the magnetic field line to itself after a circular turn starting from it, δL_X in Fig. 2, becomes very small as approaching the X point. The MHD energy minimization can take the perpendicular wavelength to be less than δL_X . However, there is an applicability limitation of MHD description. When δL_X is less than the ion Larmor radius, one cannot use the MHD theory. Therefore, in the dual-poloidal-region q description, the poloidally core region can be treated by the ideal MHD for the peeling-ballooning type of modes (or external kink modes), but the vicinity of X point Θ_X non-ideal MHD description is required. The requirement of nonideal MHD description is not just for the dual-poloidal-region q description. It is a general requirement for X-point physics. Note that the X-point singularity effect on q is spread over the magnetic surface in the surface-averaged q description and the ideal MHD codes based on the surface-averaged q requires to minimize the energy in each interval between two neighboring rational surfaces. This type of codes in principle cannot even handle the poloidally core region because

the distance between the resonant surfaces is less than the Larmor radius.

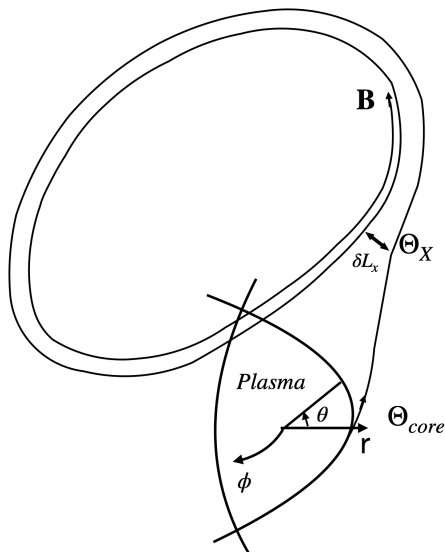


FIG. 2: Schematic plot of the magnetic field line pattern in an equilibrium with X points. The coordinate system (r, θ, ϕ) are shown, where r is the minor radius from the magnetic axis, θ is the poloidal angle, and ϕ denotes the axisymmetric toroidal angle.

To display the actual features of local q in the poloidal direction, the Solovév equilibrium is examined in this work.¹⁴ It indeed indicates that the local q tends to infinity only in the vicinity of X points. This leads us to develop the flux coordinates with dual-poloidal-region safety factor q on a magnetic surface, which describes separately the local safety factor in the vicinity of X point (Θ_X) and elsewhere in the poloidally core regions (Θ_{core}). In this coordinate system, the infinite or large local safety factor appears only in the vicinity of X points, while the local safety factor remains finite elsewhere.

With the dual-poloidal-region q coordinates, the X-point effects on the MHD modes at tokamak edge are revisited in this work. Since the X-point effects mainly affect the edge region, the modes localized at the tokamak edge are particularly examined. Two types of magnetohydrodynamic modes are studied in this description. The first is related to the conventional peeling or peeling-ballooning modes including the external kink modes. The presence of X points is confirmed to contribute a stabilizing effect for the conventionally treated modes with the surface-averaged q and with the tokamak edge portion truncated. The other is the $n = 0$ axisymmetric modes localized in the vicinity of X point, which can affect the edge transport picture near the X points. The former determines the perturbation filaments as observed in MAST.¹⁵ The latter can affect the cross field line transport in the divertor region.^{17–19} It is pointed out that the existence of axisymmetric modes may be exploited to mitigate the edge localized modes by applying sim-

ply axisymmetric resonance magnetic fields near the X points.

The manuscript is organized as follows. In Sec. II, the safety factor features in the Solovév equilibria; In Sec. III, dual-poloidal-region safety factor coordinates are developed; In Sec. IV, the X-point effects on the ideal MHD modes are investigated; In Sec. V, the conclusions and discussion are presented.

II. SAFETY FACTOR FEATURES IN THE SOLOVÉV EQUILIBRIA

To study the X-point effects on MHD modes, several equilibrium models have been used for example in Refs. 5 and 6, as well as the so-called $s - \alpha$ model.³ In these models, the equilibria with X points are constructed semi-analytically. In this work, we use the Solovév equilibria.¹⁴ The Solovév solution can approximate the DIII-D-like cross-section. For our investigation, the main concern is the profile of local safety factor (the local field line pitch) in the poloidal direction. This is mainly related to the Jacobian behavior near the X point. The Solovév equilibrium solution is sufficient to explain the situation.

For axisymmetric tokamak configuration, the magnetic field can be expressed as follows

$$\begin{aligned} \mathbf{B} &= \nabla\phi \times \nabla\chi + f(\chi)\nabla\phi \\ &= \nabla\phi \times \nabla\chi + q(\chi)\nabla\chi \times \nabla\theta_p. \end{aligned} \quad (1)$$

Here, χ is the poloidal magnetic flux, ϕ is the toroidal angle, f denotes the poloidal current density flux, $q(\chi)$ denotes the safety factor, and θ_p is the poloidal angle in the so-called PEST coordinates,²⁰ which is defined as follows

$$\begin{aligned} \theta_p &= \frac{f}{q} \int_0^{\theta_{eq}} d\theta_{eq} \frac{\mathcal{J}}{X^2}, \\ q &= \frac{f}{2\pi} \oint d\theta_{eq} \frac{\mathcal{J}}{X^2} \equiv \frac{f}{2\pi} \oint d\theta_{eq} q_{local}, \end{aligned} \quad (2)$$

$$\mathcal{J} = \frac{1}{\nabla\phi \times \nabla\chi \cdot \nabla\theta_{eq}}, \quad (3)$$

Here, θ_{eq} is the poloidal angle specified in the equilibrium code and the local safety factor $q_{local} = f\mathcal{J}/X^2$.

The Grad-Shafranov equation in cylindrical coordinates (X, Z, ϕ) is

$$X \frac{\partial}{\partial X} \frac{1}{X} \frac{\partial \chi}{\partial X} + \frac{\partial^2 \chi}{\partial Z^2} = -\mu_0 P'_X X^2 - f f'_X,$$

where P is the pressure, X is the major radius, Z is the height, μ_0 is the magnetic constant, and the prime denotes the derivative with respect to χ . In the Solovév solution, it is assumed that

$$-\mu_0 P'_X = a \quad \text{and} \quad -f f'_X = b X_0^2,$$

where X_0 is the major radius of magnetic axis. The exact Solovév equilibrium solution is then given as follows¹⁴

$$\chi = \left[(b + c_0)X_0^2 + c_0(X^2 - X_0^2) \right] \frac{Z^2}{2} + \frac{1}{8}(a - c_0)(X^2 - X_0^2)^2, \quad (4)$$

where a , b , and c_0 are constant parameters.

We first determine the separatrix of the solution in Eq. (4). This can be obtained by the stationary points of χ :

$$\begin{aligned} \frac{\partial \chi}{\partial Z} = 0 &\rightarrow X^2 - X_0^2 = -\frac{b + c_0}{c_0} X_0^2, \\ \frac{\partial \chi}{\partial (X^2 - X_0^2)} = 0 &\rightarrow Z^2 = -\frac{1}{2} \frac{a - c_0}{c_0} (X^2 - X_0^2). \end{aligned}$$

Therefore, given the X-point coordinates (X_s, Z_s) , one can determine the parameters

$$\frac{a}{c_0} = 1 - 2 \frac{Z_s^2}{X_s^2 - X_0^2}, \quad \frac{b}{c_0} = -1 - \frac{X_s^2 - X_0^2}{X_0^2}.$$

To be specific, we choose $X_0 = 3$, $X_s = 2.33$, $Z_s = 1$, and the beta at the magnetic axis $\beta_0 = 0.03$. The equilibrium cross sections are plotted in Fig. 3, with the β and f profiles given in Fig. 4. From Eq. (4) one can see that c_0^2 can be absorbed into the definitions of a and b . We therefore choose $c_0 = 1$ for simplicity. In this case, $a = 1.5601$ and $b = -0.6032$. Here, it should be pointed out that in determining f from b there is an integration constant, which is actually related to the magnitude of toroidal field. The integration constant is therefore used to scale the beta value at the magnetic axis as in Ref. 21.

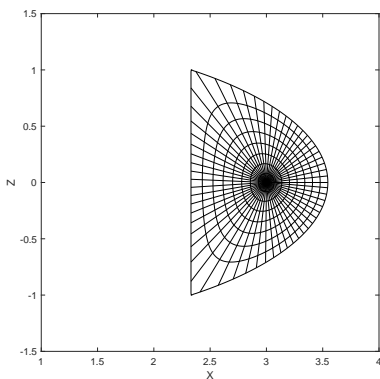


FIG. 3: The equilibrium cross section of the Solovév solution.

The safety factor can be computed for the equilibria shown in Fig. 3. The results are plotted in Fig. 5. Because at the X point, $|\nabla\chi|$ vanishes. The Jacobian in

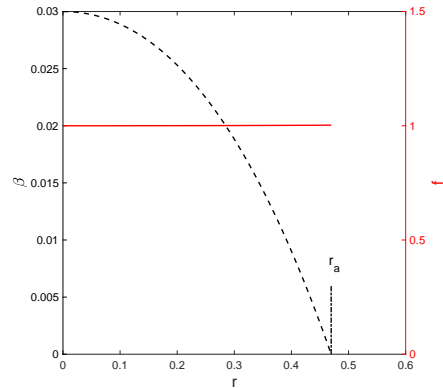


FIG. 4: The local β (black, dashed) and f (red, solid) profiles versus the minor radius (r) on the mid-plane on the out board side for the configuration as described in Fig. 3. Here, r_a indicates the plasma boundary.

Eq. (3) becomes infinite. Consequently, as is well known the surface-averaged safety factor becomes infinite on the last closed flux surface as shown in Fig. 5. From the definition of the safety factor in Eq. (2) one can see that the safety factor is a surface-averaged quantity. Noting that the Jacobian only becomes singular at the X points, one can expect that the integrand in the definition of safety factor, Eq. (2), is not singular everywhere. This leads us to plot out the local safety factor profiles, q_{local} , in Fig. 6. From Fig. 6 one can see that the surface-averaged q alone as shown in Fig. 5 may not completely describe the X-point effects on the MHD modes. The local q depends on the poloidal location. This leads us to introduce the dual-poloidal-region q description in this work in the following sections.

In the current effort, the reasons for using the Solovév equilibrium are as follows. First, the current work is the first one using the dual-poloidal-region q description. The analytical equilibrium allows others in our field to consider this approach and benchmark the results. Second, for the next efforts to include the nonideal MHD description in Θ_X and match the solutions between Θ_{core} and Θ_X regions, the analytical equilibrium simplifies the task a lot. The underlying physics of the mathematical treatment in the dual-poloidal region q description is unchanged with the Solovév analytical equilibrium. The method is applicable to the realistic equilibria, which is proposed for future studies, perhaps after the non-ideal MHD description of Θ_X region is developed. There seems to be no natural value for choosing Θ_X . As will be seen in Sec. IV C, the choice of Θ_X bears a similar effect to where to cut the edge portion in the conventional treatment based on the surface-averaged q in the ideal MHD description.²⁵

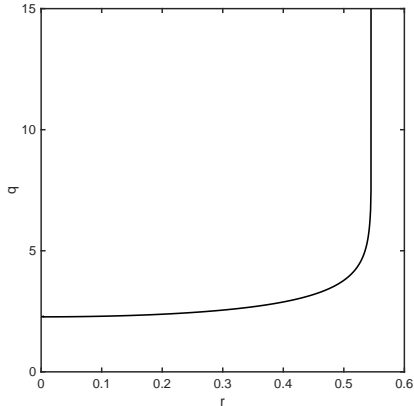


FIG. 5: The surface-averaged safety factor q profiles versus the minor radius on the mid-plane on the low field side for the configuration described in Fig. 3.

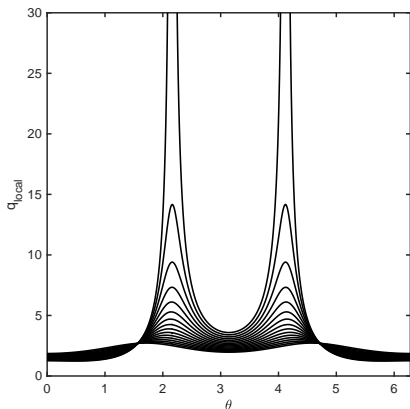


FIG. 6: The local safety factor (q_{local}) profiles versus the poloidal angle for the configuration described in Fig. 3. The consecutive q_{local} are plotted from the plasma center to the edge.

III. DUAL-POLOIDAL-REGION SAFETY FACTOR COORDINATES

In this section, we describe the flux coordinates with dual-region safety factor in the poloidal direction. The motivation for this has been discussed in Sections I and II. Instead of using the conventional flux coordinates with a surface-averaged safety factor q , the safety factor is defined according to the proximity to the X point in the edge region of plasma torus, where the equilibrium Jacobian becomes large in the local region where $|\nabla\chi|$ becomes small.

We first describe the dual-poloidal-region q coordinates in the PEST coordinates. The general flux coordinates

will be described afterward. Unlike the conventional flux coordinates in Eq. (1), the magnetic field is represented as follows

$$\begin{aligned} \mathbf{B} &= \nabla\phi \times \nabla\chi + f(\chi)\nabla\phi \\ &= \nabla\phi \times \nabla\chi + \frac{f\mathcal{J}_{eq}}{X^2}\nabla\chi \times \nabla\theta_{eq} \\ &\equiv \nabla\phi \times \nabla\chi + q_{local}(\chi, \theta_{eq})\nabla\chi \times \nabla\theta_{eq}, \end{aligned} \quad (5)$$

where $q_{local}(\chi, \theta_{eq}) \equiv f\mathcal{J}_{eq}/X^2$ represents the local safety factor. Here, it is noted that q_{local} depends on the choice of θ . To introduce the dual-poloidal-region q coordinate system, we note that Eq. (5) can be rewritten as

$$\mathbf{B} = \nabla\phi \times \nabla\chi + \frac{f\hat{\mathcal{J}}_{eq}}{X^2}h(\chi, \theta_{eq})\nabla\chi \times \nabla\theta_{eq}, \quad (6)$$

where

$$\hat{\mathcal{J}}_{eq} = \begin{cases} \mathcal{J}_{eq} = \frac{1}{\nabla\chi \times \nabla\theta_{eq} \cdot \nabla\phi}, & \theta_{eq} \in \Theta_{core}; \\ \mathcal{J}_{eq}^{max} = const. & \theta_{eq} \in \Theta_X. \end{cases}$$

$$h(\chi, \theta_{eq}) = \begin{cases} 1, & \theta_{eq} \in \Theta_{core}; \\ \frac{\mathcal{J}_{eq}}{\mathcal{J}_{eq}^{max}}, & \theta_{eq} \in \Theta_X. \end{cases}$$

Here, \mathcal{J}_{eq}^{max} is a constant and specifies the maximum allowed value for Jacobian. Since the singularity of safety factor results from the Jacobian, we limit its maximum \mathcal{J}_{eq}^{max} to pick out the vicinity of the singular point with the boundary of Θ_X defined by the poloidal angle where $\mathcal{J}_{eq} = \mathcal{J}_{eq}^{max}$. Since Jacobian varies both in χ and θ_{eq} , Θ_X depends on χ as well. Using $\hat{\mathcal{J}}_{eq}$ to define the flux coordinates of PEST type, instead of \mathcal{J}_{eq} , one obtains

$$\mathbf{B} = \nabla\phi \times \nabla\chi + q_c(\chi)h(\chi, \theta_c)\nabla\chi \times \nabla\theta_c, \quad (7)$$

where

$$\theta_c = \frac{f}{q_c} \int_0^{\theta_{eq}} d\theta_{eq} \frac{\hat{\mathcal{J}}_{eq}}{X^2}, \quad (8)$$

$$q_c(\chi) = \frac{f}{2\pi} \int_0^{2\pi} d\theta_{eq} \frac{\hat{\mathcal{J}}_{eq}}{X^2}. \quad (9)$$

Here, we have used Eq. (8) for $\theta_c(\theta_{eq})$ to transform $h(\chi, \theta_{eq})$ to $h(\chi, \theta_c)$. Equation (7) expresses the magnetic field in the dual-poloidal-region q coordinates (χ, θ_c, ϕ) . In the poloidally core region Θ_{core} , the coordinate system (χ, θ_c, ϕ) becomes the straight-field-line flux coordinates with the finite safety factor $q_c(\chi)$ being a function of χ only as in Eq. (1). In the vicinity of X point Θ_X , the local safety factor becomes $q_{local} = q_c(\chi)h(\chi, \theta_c)$, which is a function of χ and θ_c . Therefore, the dual-poloidal-region q coordinates are different from the conventional single q coordinates given in Eq. (1) but are one of the general coordinate system given in Eq. (5). Note here that since the Jacobian, $\hat{\mathcal{J}}_{eq}$, is defined according to the given \mathcal{J}_{eq}^{max} , which determines Θ_X , the parameters $\theta_c, q_c,$

and h in the dual-poloidal-region q coordinates depend on \mathcal{J}_{eq}^{\max} or Θ_X .

Now, let us describe the conversion to the general flux coordinates of dual-poloidal-region q . Letting

$$\zeta_{gc} = \phi + \nu_{eq}(\chi, \theta_c) \quad \text{and} \quad \theta_{gc} = \theta_c + \nu_{eq}(\chi, \theta_c)/(q_c h),$$

one has

$$\begin{aligned} \nabla\phi \times \nabla\chi &= \nabla\zeta_{gc} \times \nabla\chi - \frac{\partial\nu_{eq}}{\partial\theta_c} \nabla\theta_c \times \nabla\chi, \\ q_c h(\chi, \theta_c) \nabla\chi \times \nabla\theta_c &= q_c h \nabla\chi \times \nabla\theta_{gc} \\ &\quad - \frac{\partial\nu_{eq}}{\partial\theta_c} \nabla\chi \times \nabla\theta_c, -\nu_{eq} h \frac{\partial}{\partial\theta_{gc}} \left(\frac{1}{h} \right) \nabla\chi \times \nabla\theta_{gc}. \end{aligned}$$

Here, ν_{eq} is an arbitrary periodic function of θ_c . One can specify it according to the specific coordinates to be chosen, such as the Hamada or Boozer coordinates.³¹ Therefore, the magnetic field in Eq. (7) can be transformed to

$$\mathbf{B} = \nabla\zeta_{gc} \times \nabla\chi + q_c h_g(\chi, \theta_{gc}) \nabla\chi \times \nabla\theta_{gc},$$

where

$$h_g(\chi, \theta_{gc}) = \begin{cases} 1, & \theta_{gc} \in \Theta_{core}; \\ \frac{\mathcal{J}_{eq}}{\mathcal{J}_{eq}^{\max}} \left[1 + \frac{\nu_{eq}}{q_c} \frac{\partial}{\partial\theta_{gc}} \left(\frac{\mathcal{J}_{eq}^{\max}}{\mathcal{J}_{eq}} \right) \right], & \theta_{gc} \in \Theta_X. \end{cases}$$

Next, let us discuss why we introduce the dual-poloidal-region q coordinates. From the definition of surface-averaged q in Eq. (2) one can see that the integrand (\mathcal{J}) becomes infinite only at X points. It is the average that makes q become infinite everywhere on the last closed flux surface. Mathematically, we know that the singular point should be isolated with a subtle treatment, instead of being averaged to spread it. In our field, we often see this type of treatments, for example, the singular layer theory for treating the resonance surfaces.²²⁻²⁴ The dual-poloidal-region q coordinate treatment is an effort in this direction.

Note that if one uses the magnetic field representation with the surface-averaged q as given in Eq. (1), the MHD energy needs to be minimized individually in each radial interval between two neighboring resonance surfaces. Since there are infinite number of the intervals using the surface-averaged q , this makes the conventional treatment practically inapplicable for the equilibria with X points.

In the poloidal direction, the single q description leads the main harmonic to be $m_{main}^{single\ q} = nq$, which is infinite, using the Fourier decomposition method. The usual numerical scheme is aimed at minimizing the shear Alfvén energy of main harmonic for physics investigation. Being unable to treat the case with $m_{main}^{single\ q} = nq \rightarrow \infty$ just lets it to miss the physics goal for X point physics. Instead, in our dual q description the main harmonic becomes $m_{main}^{dual\ q} = nq_c$, which is finite. The finite $m_{main}^{dual\ q}$ exactly reflects the filament feature observed experimentally in Fig. 1, which are aligned to the local magnetic field.

Reference 24 gives the physics mechanism of energy minimization process, which other codes cannot avoid either as soon as the surface-averaged q alone is used. To minimize the shear Alfvén energy on a surface with infinite q , the grids have to be infinitely fine. Therefore, this issue is beyond the Fourier decomposition method. We particularly note that in the finite-element-based codes sometimes the safety factor is used as the weighting factor in the assignment of the mesh points around the resonance surfaces.⁹ In the dual-poloidal-region q coordinates, however, the singularity is forced to retreat back to the vicinity of X point, Θ_X , as it originally locates. This helps to solve the difficulty.

Besides, the surface-averaged q not only leads q become infinite as approaching to the last closed flux surface but also the magnetic shear. We know that when the magnetic shear is big, the non-ideal MHD effects, such as the FLR and resistivity effects, need to be included. This causes that even the poloidally core region, Θ_{core} , needs formally a nonideal MHD treatment in the single q description since the distance between the neighboring resonance surfaces become smaller than the Larmor radius. In fact, the local q and magnetic shear are finite in the poloidally core region Θ_{core} . The dual-poloidal-region q coordinates help to solve the difficulty and open the path to treat the poloidally core region Θ_{core} as ideal MHD, but the vicinity of X points Θ_X as nonideal MHD, and then match them together. This is another distinct feature of the dual-poloidal-region q description.

Furthermore, we point out that it has been realized before that the local safety factor diverges only in the vicinity of X points. Various MHD codes have been developed aiming at taking into consideration this specialty, for example GATO and KINX.^{9,10} Often the finite element method is used. Our approach is one of these efforts. Note that in the vicinity of X points, both the local safety factor and magnetic shear tend to infinity. In the poloidal direction, the distance between the same magnetic field lines in the different toroidal loops, δL_X , tends to zero. In the radial direction, a big magnetic shear appears. They makes the numeral approach have to have infinitely fine grids to resolve in the ideal MHD description. Note that the singular layer theory in which Mercier's criterion is derived is in principle unaffected (at least asymptotically) by the presence of X points.^{22,23,28,29} This is because theoretically one can assume the modes to be infinitely localized. However, this type of minimizations cannot be achieved numerically with finite grid density. The singular boundary layer theory in the poloidal direction for Θ_X is needed or the nonideal MHD physics needs to be added in this case. Therefore, formally isolating the Θ_X region in the dual-poloidal-region coordinates helps. The Θ_X region eventually needs the nonideal MHD description. Further discussion of dual-poloidal-region q coordinates can be found in Appendix A.

These complete the description of the dual-poloidal-region q coordinates. They will be used to study the edge localized modes in the following sections.

IV. X-POINT EFFECTS ON THE IDEAL MHD MODES

In this section, we study the X-point effects on the ideal MHD modes in tokamaks with the coordinates of dual-poloidal-region safety factor developed in Sec. III. Since the X-point effects mainly affect the edge region, the modes localized at tokamak edge are particularly examined. The magnetic field in this coordinate system can be expressed as follows

$$\mathbf{B} = \nabla\phi \times \nabla\chi + q_c(\chi)h(\chi, \theta_c)\nabla\chi \times \nabla\theta_c \quad (10)$$

$$= \mathbf{B}_c + \mathbf{B}_X, \quad (11)$$

where

$$\mathbf{B}_c = \nabla\phi \times \nabla\chi + q_c(\chi)\nabla\chi \times \nabla\theta_c, \quad (12)$$

$$\mathbf{B}_X = \begin{cases} 0, & \theta_{gc} \in \Theta_{core}; \\ q_c(\chi)(h-1)\nabla\chi \times \nabla\theta_c, & \theta_{gc} \in \Theta_X. \end{cases} \quad (13)$$

The coordinates set apart the region where the safety factor is very large, Θ_X . In the region Θ_X , the field lines are almost in the toroidal direction, i.e.,

$$\mathbf{B} \approx I\nabla\phi, \quad \theta \in \Theta_X.$$

As discussed earlier, we do not minimize the energy with the surface-averaged q coordinates. The resonance condition $m - nq = 0$ in the Fourier decomposition treatment can cause the poloidal mode number m to become infinite. To reflect that the filaments are aligned with the local magnetic field line as shown in the experiments, in this section we first consider the peeling modes in the field \mathbf{B}_c , while taking into account the \mathbf{B}_X effects in the region Θ_X . Considering \mathbf{B}_c alone in the peeling or peeling-ballooning studies resembles the conventional numerical treatment by truncating the tokamak edge portion.²⁵ As will be seen, including the additional effects from \mathbf{B}_X in the region Θ_X gives rise to the X-point stabilization effect. In the vicinity of X points, the toroidal field becomes dominant, i.e., the local q is infinite. One can imagine that the poloidally localized asymmetric modes can develop there, which will be addressed next. At the end of this section, the numerical calculation based on the code AEGIS-X is presented with the full magnetic field \mathbf{B} in Eq. (10) taken into account,²⁶ which confirms the existence of MHD filaments aligned with the local field line in the region Θ_X and the stabilization effects of X points.

A. The peeling type of modes

In this subsection, we first study the X-point effects on the peeling type of modes. To reflect the experimental observation that the filament is aligned with the local field line, to imitate the conventional treatment by truncating the edge portion, and also to avoid the modes resonating at infinite m due to using the surface-averaged

q , we will minimize the energy principle with the magnetic field \mathbf{B}_c in Eq. (12) in the whole region: Θ_{core} and Θ_X and then add the modification by \mathbf{B}_X in Eq. (13) in the vicinity of X points, Θ_X , afterward. In this way, the X-point effects are explained.

The energy principle is used for this study²⁷

$$2\delta W = \int \left\{ \frac{1}{\mu_0} \left| \delta\mathbf{B} - \mathbf{B} \frac{\mu_0 \boldsymbol{\xi} \cdot \nabla P}{B^2} \right|^2 - \frac{j_{\parallel}}{B} \boldsymbol{\xi} \times \mathbf{B} \cdot \delta\mathbf{B} - 2(\boldsymbol{\xi} \cdot \nabla P)(\boldsymbol{\xi} \cdot \boldsymbol{\kappa}) + \Gamma P(\nabla \cdot \boldsymbol{\xi})^2 \right\} d\mathbf{r}, \quad (14)$$

where $\boldsymbol{\xi}$ denotes the field line displacement, which is related to the perturbed magnetic field $\delta\mathbf{B} = \nabla \times \boldsymbol{\xi} \times \mathbf{B}$, \mathbf{j} is the equilibrium current density, $\mu_0 \delta\mathbf{j} = \nabla \times \delta\mathbf{B}$ denotes the perturbed current density, $\boldsymbol{\kappa}$ is the field line curvature, the subscripts \perp and \parallel denote the perpendicular and parallel to the equilibrium magnetic field, μ_0 is magnetic constant, the perturbed pressure $\delta P = -\boldsymbol{\xi} \cdot \nabla P - \Gamma \nabla \cdot \boldsymbol{\xi}$, Γ denotes the ratio of specific heats, and vectors are denoted by boldface.

We first consider energy minimization under the equilibrium determined by \mathbf{B}_c in Eq. (12). In this case, $\mathbf{j}_c = \nabla \times \mathbf{B}_c$ and $\nabla P_c = \mathbf{j}_c \times \mathbf{B}_c$. The minimization process is similar to the derivation of the Mercier criterion and the stability criterion for peeling modes.^{22,23,28,29} For brevity, the subscript c is omitted. Following Ref. 27, the Hamada coordinates are used with ψ and χ denoting the toroidal and poloidal magnetic fluxes, Z labeling the magnetic surfaces, and Z_0 being the reference resonance surface. We introduce the localized flux coordinates:

$$x = Z - Z_0, \quad (15)$$

$$u = \psi'(Z_0)\theta - \chi'(Z_0)\zeta. \quad (16)$$

Therefore, the parallel derivative becomes

$$\mathbf{B} \cdot \nabla = \frac{\psi'}{V'} \frac{\partial}{\partial \zeta} + \frac{\Lambda x}{V'} \frac{\partial}{\partial u}$$

with V being the volume inside a flux surface, prime denoting the derivative with respect to Z , and

$$\Lambda = \psi'(Z_0)\chi''(z_0) - \chi'(Z_0)\psi''(z_0).$$

It is also defined

$$\Theta = \frac{\nabla Z \cdot \nabla u}{|\nabla Z|^2}$$

We decompose the field line displacement as

$$\boldsymbol{\xi} = \xi \frac{\nabla Z}{|\nabla Z|^2} + \mu \frac{\mathbf{B}_c \times \nabla Z}{B_c^2} + \nu \frac{\mathbf{B}_c}{B_c^2} \quad (17)$$

and introduce the following orderings:³⁰

$$x \sim \epsilon \ll 1, \quad \frac{\partial}{\partial V} \sim \epsilon^{-1}, \quad \frac{\partial}{\partial u} \sim \frac{\partial}{\partial \zeta} \sim 1.$$

Therefore, we can further assume the following ordering scheme, which can be proved a posteriori

$$\xi = \epsilon \xi^{(1)} + \dots, \quad \mu = \mu^{(0)} + \dots, \quad \nu = \nu^{(1)} + \dots. \quad (18)$$

Here, the superscripts are used to indicate the orderings.

The minimization process for localized modes is standard.^{22,23,28,29} One can find detailed derivation in Ref. 31. One finally obtains

$$\begin{aligned} \delta W_c &= \frac{1}{2} M \omega^2 \int |\xi|^2 dx \\ &= \frac{c_0}{2} \left\{ \int \left[x^2 \left(\frac{d\xi}{dx} \right)^2 - \left(D_I + \frac{1}{4} \right) \xi^2 \right] dx \right. \\ &\quad \left. + \left(\Delta + \frac{1}{2} \right) x \xi^2 \Big|_a^b \right\}, \end{aligned} \quad (19)$$

where

$$\begin{aligned} c_0 &= \frac{\Lambda^2}{\mu_0} \frac{[\oint (dl/B)]^2}{\oint (B^2/|\nabla V|^2)(dl/B)}, \\ \Delta &\equiv \frac{1}{2} - \frac{1}{\Lambda} \left\langle \frac{\sigma B^2}{|\nabla Z|^2} \right\rangle, \\ D_I &\equiv E + F + H - \frac{1}{4}, \\ E &\equiv \frac{\langle B^2/|\nabla V|^2 \rangle}{\Lambda^2} \left(J' \psi'' - I' \chi'' + \Lambda \frac{\langle \sigma B^2 \rangle}{\langle B^2 \rangle} \right), \\ F &\equiv \frac{\langle B^2/|\nabla V|^2 \rangle}{\Lambda^2} \left(\left\langle \frac{\sigma^2 B^2}{|\nabla V|^2} \right\rangle - \frac{\langle \sigma B^2/|\nabla V|^2 \rangle^2}{\langle B^2/|\nabla V|^2 \rangle} \right. \\ &\quad \left. + P'^2 \left\langle \frac{1}{B^2} \right\rangle \right), \\ H &\equiv \frac{\langle B^2/|\nabla V|^2 \rangle}{\Lambda} \left(\frac{\langle \sigma B^2/|\nabla V|^2 \rangle}{\langle B^2/|\nabla V|^2 \rangle} - \frac{\langle \sigma B^2 \rangle}{\langle B^2 \rangle} \right), \end{aligned}$$

$\sigma = \mathbf{J} \cdot \mathbf{B}/B^2$, and $M = M_c + M_t$ with

$$\begin{aligned} M_c &\equiv \frac{\rho_m}{\alpha^2 \Lambda^2} \left\langle \frac{B^2}{|\nabla V|^2} \right\rangle \left\langle \frac{|\nabla V|^2}{B^2} \right\rangle, \\ M_t &\equiv \frac{\rho_m}{\alpha^2 \Lambda^2 P'^2} \left\langle \frac{B^2}{|\nabla V|^2} \right\rangle \left(\langle \sigma^2 B^2 \rangle - \frac{\langle \sigma B^2 \rangle^2}{\langle B^2 \rangle} \right). \end{aligned}$$

Here, it has been noted that the vacuum energy can be neglected for peeling modes as proved in Ref. 28.

After minimization of the total energy in Eq. (19) with respect to ξ , one obtains the singular layer equation

$$\frac{d}{dx} x^2 \frac{d\xi}{dx} - \left(\frac{1}{4} + D_I \right) \xi = 0. \quad (20)$$

Its solution is

$$\xi = \xi_0 |x|^{-\frac{1}{2} \pm \sqrt{-D_I}}. \quad (21)$$

Inserting Eq. (20) into Eq. (19), the energy principle is reduced to

$$\delta W_c \geq c_0 \left[\frac{x^2}{2} \left(\xi^* \frac{d\xi}{dx} + \xi \frac{d\xi^*}{dx} \right) + \left(\Delta + \frac{1}{2} \right) x |\xi|^2 \right]_{x_a}^{x_b} \quad (22)$$

Then, by inserting the solution of the singular layer equation in Eq. (21), one can find the minimum energy. Without considering the X-point contribution, the stability condition for peeling mode is just $\Delta < 0$. One needs to add the X-point effects from \mathbf{B}_X in Eq. (13) in the vicinity of X point, Θ_X .

To find out the \mathbf{B}_X effects seems to be complicated. However, we note that the region Θ_X is smaller than $\Theta_{core} + \Theta_X$ and more importantly that the minimization process for the localized modes leading to Eq. (19) has already been performed in the magnetic field described by \mathbf{B}_c . Therefore, the non-minimized Alfvén mode contribution in the first term of Eq. (14) is dominant and we only need to add the additional contribution to this term in region Θ_X .

First, we note that $\delta \mathbf{B}$ in Eq. (14) can be decomposed as

$$\begin{aligned} \delta \mathbf{B} \cdot \nabla Z &= \nabla \cdot [(\boldsymbol{\xi} \times \mathbf{B}) \times \nabla Z] \\ &= \mathbf{B} \cdot \nabla (\boldsymbol{\xi} \cdot \nabla Z), \end{aligned} \quad (23)$$

$$\begin{aligned} \frac{\delta \mathbf{B} \cdot \mathbf{B} \times \nabla Z}{|\nabla Z|^2} &= \mathbf{B} \cdot \nabla \left(\frac{\boldsymbol{\xi} \cdot \mathbf{B} \times \nabla Z}{|\nabla Z|^2} \right) \\ &\quad - \frac{\mathbf{B} \times \nabla Z}{|\nabla Z|^2} \cdot \nabla \times \frac{\mathbf{B} \times \nabla Z}{|\nabla Z|^2} \boldsymbol{\xi} \cdot \nabla Z, \end{aligned} \quad (24)$$

$$\begin{aligned} \frac{1}{B^2} \left(\delta \mathbf{B} - \mathbf{B} \frac{\mu_0 \boldsymbol{\xi} \cdot \nabla P}{B^2} \right) \cdot \mathbf{B} &= -\nabla \cdot \boldsymbol{\xi} \\ &\quad - \mathbf{B} \cdot \nabla \left(\frac{\boldsymbol{\xi} \cdot \mathbf{B}}{B^2} \right) - 2\boldsymbol{\xi} \cdot \boldsymbol{\kappa}. \end{aligned} \quad (25)$$

Here, we have considered the decompositions in the total magnetic field in Eq. (11), instead of \mathbf{B}_c , in order to take into account the extra energy from the X-point contribution.

To evaluate the $\delta \mathbf{B}$ components in Eqs. (23)-(25), we decompose the field line displacement in the minimization process with \mathbf{B}_c in Eq. (17) in the total magnetic field representation

$$\boldsymbol{\xi} = \xi_t \frac{\nabla Z}{|\nabla Z|^2} + \mu_t \frac{\mathbf{B} \times \nabla Z}{B^2} + \nu_t \frac{\mathbf{B}}{B^2}. \quad (26)$$

Equating Eqs. (17) and (26) one obtains

$$\xi_t = \xi, \quad (27)$$

$$\mu_t = \mu \frac{\mathbf{B} \cdot \mathbf{B}_c}{B_c^2}, \quad (28)$$

$$\nu_t = \nu \frac{\mathbf{B} \cdot \mathbf{B}_c}{B_c^2}. \quad (29)$$

Here, it has been noted that the poloidal magnetic field is negligible in the region Θ_X and $\mathbf{B} \cdot \mathbf{B}_c = f_{qc}/\mathcal{J}_c$.

Using Eqs. (23)-(29), one can evaluate the extra energy from the X-point effects by calculating the first term of Eq. (14). This is because the first term represents the energy of the Alfvén modes, which is one order larger than the rest terms in the singular layer theory.^{22,23} Noting that in the minimization process with \mathbf{B}_c , one has μ is one order larger than ξ and ν .^{27,31} Therefore, the extra energy from the X-point contribution becomes

$$\begin{aligned}\delta W_X &= \frac{1}{2\mu_0} \int_{\Theta_X} \left| \delta \mathbf{B} - \mathbf{B} \frac{\mu_0 \boldsymbol{\xi} \cdot \nabla P}{B^2} \right|^2 d\mathbf{r} \\ &= \frac{1}{2\mu_0} \int_{\Theta_X} \left| \frac{|\nabla Z|}{B} \mathbf{B} \cdot \nabla \left(\frac{\boldsymbol{\xi} \cdot \mathbf{B} \times \nabla Z}{|\nabla Z|^2} \right) \right|^2 d\mathbf{r} \\ &= \frac{1}{2\mu_0} \int_{\Theta_X} \left| \frac{|\nabla Z|}{B} \mathbf{B} \cdot \nabla \left(\mu_t \frac{B^2}{|\nabla Z|^2} \right) \right|^2 d\mathbf{r} \\ &= \frac{n^2}{2\mu_0} \int_{\Theta_X} \left| \frac{\mathbf{B}\mathbf{B} \cdot \mathbf{B}_c}{B_c^2 |\nabla Z|} \frac{f}{X} \mu \right|^2 d\mathbf{r}. \quad (30)\end{aligned}$$

Here, μ is related ξ in δW_c in Eq. (22) by²⁷

$$\frac{\partial \xi}{\partial x} + \frac{\partial \mu}{\partial u} = 0.$$

From the ordering analyses in Eq. (18), one can see that the integrand in δW_X in Eq. (30) is larger than that in δW_c in Eq. (22). However, the integration domain for δW_X , Θ_X , is smaller than that for δW_c , $\Theta_{core} + \Theta_X$.

The system stability is determined by the total energy

$$\delta W = \delta W_c + \delta W_X.$$

Since δW_X is positive definite, the X-point effects are shown to give rise to the stabilizing effects. The smaller the region Θ_X , the more stringent the stability condition becomes. Only when \mathbf{B} becomes parallel to \mathbf{B}_c in the limit $\Theta_X \rightarrow 0$, one has $\delta W_X = 0$. This indicates that the usual numerical treatment by truncating the tokamak edge region gives rise to an overly stringent stability condition. Smaller Θ_x implies the larger q_c . As discussed earlier in Sec. III, there is a physics and numerical limitation for approaching the surface-averaged safety factor. These phenomena will be further confirmed numerically using AEGIS-X code to be described in Sec. IV C.

B. The axisymmetric modes in the vicinity of X points

In this subsection, we discuss a special mode which can be recovered in the dual-poloidal-region q description, the axisymmetric modes in the vicinity of X points. In the surface-averaged q description, the conventional safety factor becomes infinite on the last closed flux surface. However, it does not imply the poloidal magnetic field vanishes everywhere on the last closed flux surface. Actually, the local q in the poloidally core region, Θ_{core} remains finite. The magnetic field becomes basically the

toroidal field only in the vicinity of X points in the region Θ_X . Because the magnetic field is about along the toroidal direction in Θ_X , in view of the minimization of the field line bending effects one may expect that the $n = 0$ localized axisymmetric modes can develop in this region. Mathematically, this situation is well described by the dual q coordinates. From the description of the dual-poloidal-region q coordinates in Sec. III one can see that $h = 1$ in Θ_{core} and $h = \mathcal{J}_{eq}/\mathcal{J}_{eq}^{\max}$ in Θ_X . This makes $q_c h$ become q_{local} in the vicinity of X points, which is infinite. Therefore, one can carry directly the axisymmetric mode analyses in Θ_X in the dual-poloidal-region q description.

The localized stability criterion for $n = 0$ axisymmetric modes can be obtained from the conventional Mercier or peeling stability criterion, which is actually embedded in the discussion of peeling modes in Sec. IV A,

$$\begin{aligned}\delta W_c &= \frac{c_0}{2} \left\{ \int_{\Delta\Theta_X} \left[x^2 \left(\frac{d\xi}{dx} \right)^2 - \left(D_I + \frac{1}{4} \right) \xi^2 \right] dx \right. \\ &\quad \left. + \left(\Delta + \frac{1}{2} \right) x \xi^2 \Big|_a^b \right\}, \quad (31)\end{aligned}$$

where $\Delta\Theta_X$ is the region in the vicinity of X point where the axisymmetric perturbation is considered,

$$\begin{aligned}c_0 &= \frac{\Lambda^2}{\mu_0} \frac{[\mathcal{f}(dl/B)]^2}{\mathcal{f}(B^2/|\nabla V|^2)(dl/B)} \\ &\approx \frac{2\pi X_X \Lambda^2 |\nabla V|^2}{\mu_0 B^3}, \quad (32)\end{aligned}$$

$$\Delta \equiv \frac{1}{2} - \frac{1}{\Lambda} \left\langle \frac{\sigma B^2}{|\nabla Z|^2} \right\rangle \approx \frac{1}{2} - \frac{1}{\Lambda} \frac{\sigma B^2}{|\nabla Z|^2}, \quad (33)$$

$$D_I \equiv E + F + H - \frac{1}{4}, \quad (34)$$

$$\begin{aligned}E &\equiv \frac{\langle B^2/|\nabla V|^2 \rangle}{\Lambda^2} \left(J' \psi'' - I' \chi'' + \Lambda \frac{\langle \sigma B^2 \rangle}{\langle B^2 \rangle} \right) \\ &\approx \frac{B^2/|\nabla V|^2}{\Lambda^2} (J' \psi'' - I' \chi'' + \Lambda \sigma), \quad (35)\end{aligned}$$

$$\begin{aligned}F &\equiv \frac{\langle B^2/|\nabla V|^2 \rangle}{\Lambda^2} \left(\left\langle \frac{\sigma^2 B^2}{|\nabla V|^2} \right\rangle - \frac{\langle \sigma B^2/|\nabla V|^2 \rangle^2}{\langle B^2/|\nabla V|^2 \rangle} \right. \\ &\quad \left. + P'^2 \left\langle \frac{1}{B^2} \right\rangle \right) \approx \frac{P'^2}{\Lambda^2/|\nabla V|^2}, \quad (36)\end{aligned}$$

$$\begin{aligned}H &\equiv \frac{\langle B^2/|\nabla V|^2 \rangle}{\Lambda} \left(\frac{\langle \sigma B^2/|\nabla V|^2 \rangle}{\langle B^2/|\nabla V|^2 \rangle} - \frac{\langle \sigma B^2 \rangle}{\langle B^2 \rangle} \right) \\ &\approx 0 \quad (37)\end{aligned}$$

with X_X being the major radius of X point. Here, it has been considered that the equilibrium is axisymmetric, the poloidal magnetic field about vanishes, and the poloidally localized $n = 0$ modes are considered. In this case, the average $\langle \cdot \rangle$ here represents the average over a toroidal loop. The Pfirsch-Schlüter current is negligible

and the parallel current density σ is dominated by the axisymmetric Ohmic current in the vicinity of X points.

Like the Mercier criterion, the stability condition just indicates the condition of mode existence. Since $q_{local} \rightarrow \infty$, the field lines in the region Θ_X just run toroidally. In this case, the stability criterion reduces to the conventional flux-tube-like analyses for interchange modes with magnetic shear taken into account. Besides the physical interpretation of E , F , and H representations in Ref. 30 and the expressions in a tokamak with a large aspect ratio and circular cross section in Ref. 32, we use an alternative approach to show the existence condition of the axisymmetric modes. Note that Eq. (34) can be alternatively written as^{33,34}

$$D_I = \frac{\langle g \rangle}{\langle \mathbf{B} \cdot \nabla \Lambda_s \rangle^2} \left[\langle P' \kappa_n \rangle + \left\langle \mathbf{B} \cdot \nabla \Lambda_s \left(\lambda_c - \frac{\langle g \lambda_c \rangle}{\langle g \rangle} \right) \right\rangle \right. \\ \left. + \left\langle g \left(\lambda_c^2 - \frac{\langle g \lambda_c \rangle^2}{\langle g \rangle^2} \right) \right\rangle \right] - \frac{1}{4}, \quad (38)$$

where

$$g = \frac{B^2}{|\nabla \chi|^2}, \quad \kappa_n = \frac{2 \nabla \chi \cdot \boldsymbol{\kappa}}{|\nabla \chi|^2}, \\ \kappa_g = \frac{\mathbf{B} \times \nabla \chi \cdot \boldsymbol{\kappa}}{B^2}, \quad \mathbf{B} \cdot \nabla \lambda_c = \mu_0 P' \kappa_g, \\ \mathbf{B} \cdot \nabla \Lambda_s = -\frac{1}{|\nabla \chi|^4} (\mathbf{B} \times \nabla \chi) \cdot \nabla \times (\mathbf{B} \times \nabla \chi).$$

Here, we have kept the notations in Ref. 34. The formulas to prove the equivalence between Eqs. (34) and (38) can be found in Ref. 31 with $\lambda_c = \sigma/2$. In the localized axisymmetric mode limit in the vicinity of X point, Eq. (38) is reduced to

$$D_I \approx \frac{g \mu_0 P' \kappa_n}{(\mathbf{B} \cdot \nabla \Lambda_s)^2} - \frac{1}{4}. \quad (39)$$

Note further that the magnetic shear parameter can be reduced to

$$\mathbf{B} \cdot \nabla \Lambda_s \\ = -\frac{1}{|\nabla \chi|^4} (\mathbf{B} \times \nabla \chi) \cdot \nabla \times [(q_c h \nabla \chi \times \nabla \theta_c) \times \nabla \chi] \\ \approx \frac{1}{|\nabla \chi|^4} \nabla(q_c h) \times (\mathbf{B} \times \nabla \chi) \cdot [(\nabla \chi \times \nabla \theta_c) \times \nabla \chi] \\ = \frac{\mathbf{B} \cdot \nabla \theta_c}{|\nabla \chi|^2} \nabla \chi \cdot \nabla(q_c h).$$

The physical meaning is obvious here. The term $g P' \kappa_n$ denotes the well-known magnetic well effect. The term $1/4$ is related to the magnetic shear $(\mathbf{B} \cdot \nabla \Lambda_s)^2$ as relatively compared with the first term on the right-hand side of Eq. (39).

In the ordering analyses in Eq. (B3) in Appendix B, we show that the first term on the right-hand side of Eq. (39) becomes

$$\frac{g \mu_0 P' \kappa_n}{(\mathbf{B} \cdot \nabla \Lambda_s)^2} \sim (X_s^2 \mu_0 / B^2) \boldsymbol{\kappa} \cdot \nabla p. \quad (40)$$

The stability condition in Eq. (39) indicates that the estimate in Eq. (40) should be larger than $1/4$ for the instability to occur in the ideal MHD description. It may happen. However, the condition is high especially as compared with the resistive MHD case. When the resistivity is taken into account, one can expect that the $n = 0$ resistive interchange and tearing modes can develop on the bad curvature side in the vicinity of X point.³⁰ As proved by the well-known theory in Ref. 30, when the resistivity effects are taken into account, the magnetic shear stabilization term, i.e., the term “ $1/4$ ” (which is related to $(\mathbf{B} \cdot \nabla \Lambda)^2$), in Eq. (39) disappears. This causes the resistive modes to develop as soon as $\boldsymbol{\kappa} \cdot \nabla p > 0$ in the vicinity of X points.

The localized axisymmetric modes can be understood by comparing a tokamak scenario without a toroidal current to generate the poloidal magnetic field for field line rotational transform $1/q$, which is unstable to the interchange modes on the low field side in this case. Tokamak stability relies on the average magnetic well, which is induced by the finite safety factor. The difference for the localized axisymmetric modes is that there is a large magnetic shear in the vicinity of X points. However, the resistivity can delete the shear stabilization effects.³⁰ Therefore, the localized axisymmetric modes can potentially develop in the vicinity of X points.

Furthermore, noting the axisymmetric mode feature, one can potentially apply the $n = 0$ or high m/n resonance magnetic perturbation in the region near the X point to enhance the X-point transport to mitigate ELMs. Note that we are discussing the axisymmetric RMP, an external drive here. It does not necessarily require the high m axisymmetric modes to be unstable. It can happen when the magnetic field patterns coincide. In fact, neither the conventional $n \neq 0$ RMP is considered to resonate with the peeling-ballooning modes at the pedestal. Instead, the finite m/n magnetic field pattern resonance is considered. Engineeringly, this can be an alternative the current finite m/n RMP approach. One can also expect that the current dual-poloidal-region q description can affect the understanding of the cross field line transport in the divertor region.^{17,18}

C. X-point effects on the external kink modes

In the subsections IV A and IV B, we have demonstrated the X-point effects on the localized modes analytically. In this subsection, we show the numerical results about the existence of the modes aligned with the local magnetic field lines in the poloidally core region, Θ_{core} , and the X-point effects on them. The numerical treatment allows us to include the coupling of multiple Fourier components to actually deal with the external kink modes. It is noted that in the later peeling-ballooning mode computations, the external kink modes are sometimes grouped into the low n peeling-ballooning modes. This is an extension of the analytical theory for

peeling modes in Sec. IV A. The axisymmetric modes described in Sec. IV B are trivial to understand and therefore are not specially needed to have a numerical demonstration in the current status.

We extend the AEGIS code²⁶ to AEGIS-X for this study by numerically solving the MHD equation as follows

$$-\rho_m \omega (\omega - \omega_*) \boldsymbol{\xi}_\perp = \delta \mathbf{J} \times \mathbf{B} + \mathbf{J} \times \delta \mathbf{B} - \nabla \delta P.$$

Here, for simplicity we consider only incompressible plasma, i.e., ignoring the coupling of parallel motion. One reason for this also is because the connection length between the good and bad curvature regions varies significantly from the poloidally core (Θ_{core}) to X point (Θ_X) regions. More subtle kinetic treatment for parallel motion is required in this case. This is beyond the current MHD framework. We do include the ion diamagnetic drift effect, ω_* , in the inertia term. This can suppress the high m harmonic coupling.

In AEGIS,²⁶ the Fourier decomposition method is used in the poloidal direction, which precludes numerically including the diverted surface like other codes based on the Fourier decomposition method. In the radial direction, the decomposition based on the independent solution method is used. The adaptive shooting method is then used to obtain the independent solutions. The conventional general flux coordinates with the surface-averaged q are used in the AEGIS code. In the presence of X points, the safety factor tends to infinity on the last closed flux surface. One may be able to minimize the field line bending effects in the general straight field line coordinates. However, the minimization of resonance effects, $m - nq = 0$, leads the poloidal mode number to become infinite. This is certainly unacceptable in numerical treatment for MHD description. Noting that infinite local q actually occurs only in the vicinity of X points, the dual-poloidal-region q coordinates were developed in Sec. III. In extending the AEGIS to AEGIS-X from the surface-averaged q to the dual-poloidal-region q coordinates, the following change is made

$$q(\chi)|_{AEGIS} \rightarrow q_c(\chi)h(\chi, \theta)|_{AEGIS-X}$$

In AEGIS-X, the transformation of $q_c(\chi)h(\chi, \theta)$ to a matrix in the Fourier space is performed.

In this formulation, the magnetic field is expressed in Eq. (7), which is the complete representation. Because of the dual-poloidal-region q coordinates are used, the difficulty of infinite resonance surfaces in the conventional surface-averaged q description is avoided.

We keep using the Solovév equilibrium to demonstrate the X-point effects on the external kink modes. To be specific, we discuss the equilibrium with $\beta = 0.03$, $X_0 = 3$, $X_s = 2.33$, and $Z_s = 1$ as shown in Figs. 3-6. In the dual-poloidal-region q coordinates, there is an assumption on where the maximum Jacobian is imposed. This is a parameter beyond what the MHD theory can fully determine. Note that the cutting-off of the maximum Jacobian corresponds to limiting the edge safety

factor with the magnetic field \mathbf{B}_c . We, therefore, scan various cutting-off positions, with q_c at edge ($q_{c,a}$) ranging from 5.8 to 7.2. The smaller $q_{c,a}$, the larger Θ_X . Figure 7 shows the surface-averaged q profile together with the q_c profiles for the cases with the edge safety factor $q_{c,a} = 6.0$ and 7.0 respectively. To see the safety factor feature, the function $h(\chi, \theta)$ for the case $q_{c,a} = 6.8$ is plotted in Fig. 8.

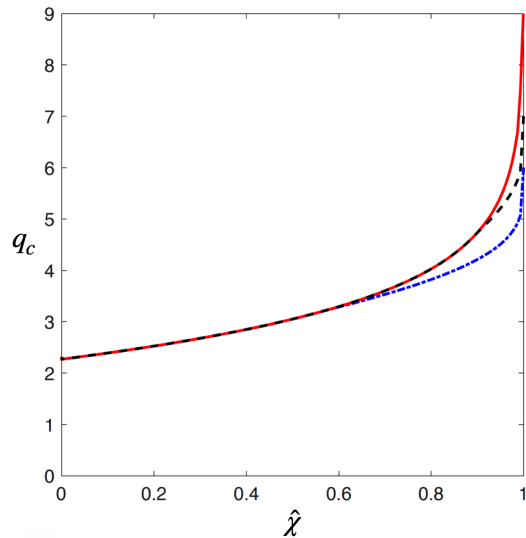


FIG. 7: The safety factor profiles versus the normalized poloidal flux. The red curve corresponds to the surface-averaged q , which tends to infinity at $\hat{\chi} = 1$, the dashed and dot-dashed blue curves correspond respectively to q_c in the cases with $q_{c,a} = 7$ and 6 .

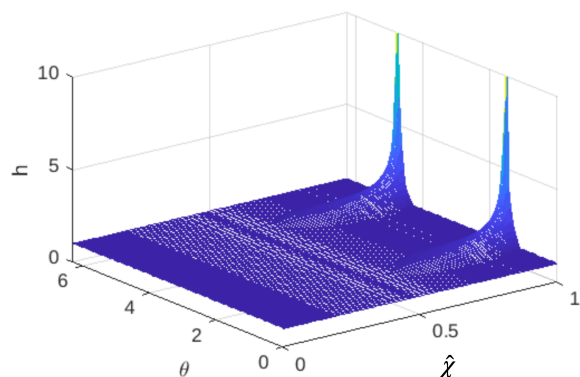


FIG. 8: The typical h profile versus $\hat{\chi}$ and θ_c . In this plot, $q_{c,a} = 6.8$ at $\hat{\chi} = 1$.

The $n = 1$ modes are studied in the dual-poloidal-region q coordinates. Fig. 9 shows the critical wall positions for the cases with $q_{c,a} = 5.8, 6.0, 6.2, 6.8, 7.0$, and 7.2

with the conformal wall. The system is stable if the perfectly conducting wall is placed within the critical wall position, otherwise unstable. Therefore, the system is more stable with a larger critical wall position. In the calculation, the coordinates (χ, θ_c, ϕ) with dual-poloidal-region q are used. Therefore, we are able to study the modes aligned with the local magnetic field lines. The existence of this type of modes is confirmed, The typical eigenmode in the dual-poloidal-region q coordinates is given in Fig. 10 for the case with $q_{c,a} = 6.8$.

From Fig. 9 one can see that the larger $q_{c,a}$ in the overall trend the more unstable the system becomes. Note that the larger $q_{c,a}$ corresponds to the smaller Θ_X . This indicates that the smaller the angle Θ_X in the overall trend, the more unstable the numerical results indicate. This is consistent with the analytical theory for peeling modes in Sec. IV A.

We have not reduced Θ_X further in the numerical calculation to determine the most stringent stability condition in the ideal MHD description. As discussed earlier in Sec. III in discussing why we introduce the dual q coordinates, further reduction in Θ_X would place the current treatment beyond the applicability limit of MHD description. In the poloidal direction, the distance between the same magnetic field lines in the different toroidal loops, δL_X in Fig. 2 tends to be zero. In the radial direction, a big magnetic shear appears. The kinetic effects become significant in the Θ_X region for external kink modes. Furthermore, since the toroidal current density is constant in the Solovév equilibrium, which extends to the plasma edge, one needs infinitely fine grids or infinite number of poloidal Fourier components to minimize the field-line-bending energy, which is beyond the numerical code capacity. For these reasons, we only display the tendency of stability criterion with respect to Θ_X at the current stage. We will consider this limit when full kinetic/resistive effects are taken into account.

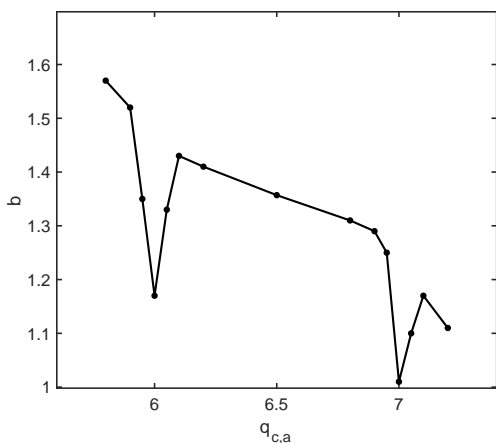


FIG. 9: The critical wall positions versus the edge safety factor $q_{c,a}$ in the dual-poloidal-region coordinates.

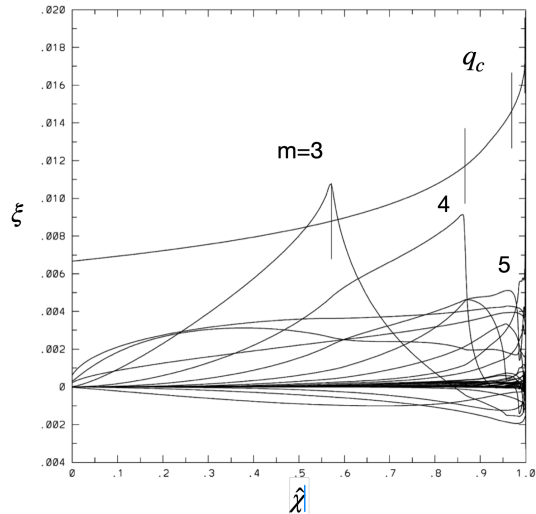


FIG. 10: The typical eigenfunction. The plot corresponds to the case with $q_{c,a} = 6.8$.

From Fig 9, one can also see a typical feature of the peeling type of modes. The stability condition becomes more stringent whenever the resonance surface falls exactly on the plasma-vacuum interface. The critical wall position has a minimum when $q_{c,a}$ is an integer. Similar phenomena have been observed in the cases with the edge portion truncated.²⁵

V. CONCLUSIONS

In this paper, the X-point effects on the ideal MHD modes in tokamaks are investigated using the dual-poloidal-region q coordinates. Since the X point effects mainly affects the edge region, the modes localized at tokamak edge are particularly examined. The procedure is an alternative to the finite element method used in this field.

Since the dual-poloidal-region safety factor is introduced, this makes our approach consistent with the experimental observation that the filaments are aligned with the local field lines in the poloidally core region, Θ_{core} . Indeed, from the analyses of the local safety factor using the Solovév equilibrium, it is confirmed that the local safety factor actually tends to infinity only in the vicinity of X points, while it remains finite elsewhere. Therefore, we conclude that the surface-averaged q alone does not reflect the subtle feature of field line pitch. The coordinates based on the dual-poloidal-region q can catch the subtle feature of the tokamak edge localized modes in the presence of X points.

Two types of magnetohydrodynamic modes are studied using the dual-poloidal-region q coordinates both analytically and numerically. Using the dual q coordinates, we first prove that the X point effects can provide a stabiliz-

ing effect on the modes localized at tokamak edge by the singular mode theory,^{27,30} which show that the smaller Θ_X the more unstable the system becomes. The results are confirmed in the AEGIS-X calculation. We have not considered the limit $\Theta_X \rightarrow 0$ in view of that the nonideal MHD effects can play a significant role in the vicinity of X points. The existence of the modes aligned with the local magnetic field in the core region Θ_{core} is confirmed. The analyses bear some kind of similarity with the conventional treatment with the surface-averaged q and with the edge portion truncated.

Here, we explain further that the X-point effects on the external kink modes cannot be fully resolved numerically in the ideal MHD description. Neither our dual q code nor existing ideal MHD codes can achieve the “converged results” for X point effects in the ideal MHD framework regardless of the numerical method used. The reasons are summarized here. To minimize the stabilizing energy from the field line bending effects, the pressure gradient modes in the lowest order tend to become flux-tube-like. The flux tube with finite perpendicular size in the poloidally core region Θ_{core} evolves into an infinitely thin sheet as it approaches the X points. Therefore, infinite fine mesh is required to resolve the flux tube modes at the X points. This is not achievable numerically. Even if one could do it, the perpendicular wavelength near the X points would exceed the ideal MHD applicable limit. The nonideal MHD effects, such as FLR and resistive effects, can play significant roles. The dual q description paves the way to include the nonideal MHD effects by isolating the singularity to the vicinity of X points, which otherwise spreads over the whole surface with infinite q everywhere.

One can also see this from the derivation of Mercier’s criterion. Because the magnetic shear is infinite at the edge with X points, the scale length of radial localized modes approaches zero in the derivation of Mercier’s criterion. This infinitely fine structure can be resolved analytically but not numerically. This is why only the tendency of X point effects is shown in our numerical work in Fig. 9. Instead, in the analytical peeling mode theory in Sec. IV A, one can take the limit $\Theta_X = 0$.

Using the dual-poloidal-region safety factor, we are able to determine the condition of the existence of the axisymmetric modes localized in the vicinity of X point. The poloidal magnetic field vanishes in this region. The $n = 0$ localized modes can develop locally there if the resistivity or external RMP drive is taken into account. This has important implications. More importantly, the existence of axisymmetric modes (or the magnetic field pattern) points to the possibility of applying a toroidally axisymmetric RMP in the X-point region for mitigating the edge localized modes. This can be an alternative to the current RMP coil design in tokamaks. Here, we would like to mention the earlier research on the global vertical instabilities, for example, in Refs. 35-37. The $n = 0$ vertical modes are related to the low m modes so that the plasma column moves vertically as a whole. The current

$n = 0$ axisymmetric modes belong to the high m case, which are localized in the vicinity of X points. They are different. Nevertheless, note that in the investigation of X point effects on the global vertical instabilities, Refs. 35 and 36 pointed out that the $n = 0$ modes can have resonant effects at the X points. This can be a numerical support to the $n = 0$ RMP concept pointed out in the current paper.

The current dual q description also has important implications for the present concept of finite m/n RMPs. The double-null (DN) configurations are thought to have better power handling and performance as compared to the single-null (SN) configurations. However, the RMP ELM suppression is usually only observed in the SN configurations and there is no hint of RMP ELM suppression can be achieved in the DN configurations.⁴⁰ In the dual q (or local q) picture, one can see the reason. If RMPs are configured according to the averaged q , the deviation from the local q in the DN configurations is much larger than in the SN configurations. Taking into account the dual q feature is also important for the existing concept of finite m/n RMPs. It opens the possibility of further improving the current finite m/n RMP concept by considering the alignment to the local q . Our dual q description indicates that both RMP concepts, finite m/n and $n = 0$, have their own potential and deserve to be studied in parallel.

Nevertheless, this is the first effort to introduce the dual-poloidal-region q description. Because of the variation of connection length and the dependence of finite Larmor radius effects on the local safety factor, kinetic description^{38,39} may be needed to further clarify the edge physics. The resistivity effects can be also important in the vicinity of X points. We especially point out that in the ideal MHD description, Θ_X cannot be fully determined. The applicability of ideal MHD theory shows that there is a lower limit for Θ_X . For example, δL_x in Fig. 2 cannot be smaller than the ion Larmor radius for MHD to be physically relevant. This is because for a flux-tube type of modes, for example the interchange or ballooning modes, with a finite \mathbf{k}_\perp in the region Θ_{core} , their \mathbf{k}_\perp in the region Θ_X would become extremely large and therefore the FLR effects on them are important. Since the complete determination of Θ_X requires non-ideal MHD theory, in the current ideal MHD description, we have, nevertheless, performed a parameter scan of Θ_X and derived the analytical stability condition with Θ_X as a parameter to show the X-point stabilization. These are only for external kink modes. The nonideal MHD analyses of external kink modes or peeling-ballooning type of modes are proposed for future studies.

Actually, this is not a special issue to the current dual-poloidal-region q description, a similar or even more demanding requirement appears also in the single surface-averaged q description. The single surface-averaged q description results in indefinitely dense singular surfaces at the edge. Note that the distance of rational surfaces cannot be smaller than the Larmor radius for MHD to be

physically relevant. The single surface-averaged q treatment meets the uncertainty for where to truncate the plasma edge portion as pointed out in Ref. 25. Both cases have a common origin from the X-point singularity. As a matter of fact, the required region for nonideal MHD treatment is narrower in the dual-poloidal-region q description. In contrast, the region is spread all over the magnetic surfaces near the edge in the single surface-averaged q description.

We also point out the recent development of the X-point equilibrium research in Ref. 13. It is found that the X point actually does not exist on the plasma-vacuum interface, but in the closely nearby vacuum region. The surface-average q may not tend to be infinity at the plasma edge. But, it is still large. To study the modes aligned with the local magnetic field in the core region, the dual-poloidal-region q description is still necessary in this case.

The authors would like to acknowledge Dr. Richard Fitzpatrick for helpful discussion. This research is supported by Department of Energy Grants DE-FG02-04ER54742.

Appendix A: Features of dual-poloidal-region q coordinates

In this appendix, we discuss the features of dual-poloidal-region q coordinates as described in Sec. III.

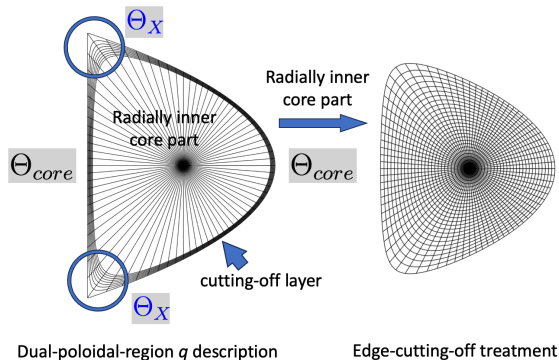


FIG. 11: Comparison between the dual-poloidal-region q description and the edge-cutting-off treatment.

In the single q description with the conventional flux coordinates, the edge q tends to be infinite. This leads considerable numerical codes based on this coordinate system to cut off some portion of edge region as shown in Fig. 11. Compared with this type of treatments, the dual-poloidal-region q coordinate system reinstates the cutting-off edge region. In the dual-poloidal-region q coordinate description, the radially inner core part is described identically as the conventional treatment by the

flux coordinates with single q , while the dual q description is introduced for the edge layer which is cut off in the conventional edge-cutting-off treatment.

If one picked up the cutting-off layer in the single q description, the q value in this layer would become infinite or rather larger. Instead, in the dual q description, the q value remains finite in the poloidally core region, Θ_{core} , and only becomes infinite or rather large in the vicinity of X points, Θ_X .

There are several advantages of dual-poloidal-region q description. First, one can see immediately that the localized axisymmetric mode may develop in the vicinity of X points, Θ_X . Second, the cutting-off treatment of external kink or peeling-ballooning modes tends to miss the stabilizing effects from δW_X . Here, it has been noted that the cutting-off treatment of external kink or peeling-ballooning modes focuses on the modes with finite m/n (i.e., around the edge safety value q_a), which cannot align with the field lines in the vicinity of X points, Θ_X . Furthermore, as pointed out in the main text, the X-point physics is intrinsically nonideal MHD. Isolating the singularity of q_{local} in Θ_X is potentially helpful for nonideal MHD treatment of X-point physics. The ‘‘singular point’’ theory may replace the conventional singular layer theory at the edge with X points.

Appendix B: Ordering analyses of $n = 0$ localized axisymmetric modes

In Sec. IV B, we have derived the stability criterion of the localized axisymmetric modes, which in the ideal MHD is given by Eq. (39). The criterion shows that the balance between the pressure gradient drive and shear stabilization effects determines the stability. Note that in the resistive MHD, the $n = 0$ localized axisymmetric modes are always unstable on the bad curvature side since the shear stabilization term disappears as proved in Ref. 30. Here, we analyze the criterion in the ideal MHD case.

Using the definitions in Sec. III, one can further reduce the first term on the right hand side of Eq. (39). Noting that

$$\begin{aligned} \mathbf{B} \cdot \nabla \theta_c &= \nabla \phi \times \nabla \chi \cdot \nabla \theta_c \\ &= \nabla \phi \times \nabla \chi \cdot \nabla \theta_{eq} \frac{\mathcal{J}_{eq}^{\max} f}{X^2 q_c} \\ &= \mathcal{J}_{eq}^{-1} \frac{\mathcal{J}_{eq}^{\max} B}{X q_c} \end{aligned}$$

and

$$q_c h = q_c \frac{\mathcal{J}_{eq}}{\mathcal{J}_{eq}^{\max}},$$

one has

$$\begin{aligned} \frac{g\mu_0 P' \kappa_n}{(\mathbf{B} \cdot \nabla \Lambda_s)^2} &= \frac{B^2 2\mu_0 \boldsymbol{\kappa} \cdot \nabla p}{(\mathbf{B} \cdot \nabla \theta \nabla \chi \cdot \nabla(q_c h))^2} \\ &= \frac{(X_s^2 2\mu_0 / B^2) \boldsymbol{\kappa} \cdot \nabla p}{[(1/B) \nabla \chi \cdot \nabla \ln \mathcal{J}_{eq}]^2}. \end{aligned} \quad (\text{B1})$$

We now estimate the denominator of Eq. (B1). Noting that at the X point $\nabla \chi = 0$, one has $\nabla \chi = B a \delta r / a$, where $\delta r / a$ is the scaled distance from the X point. Noting further that $\mathcal{J}_{eq} \sim R a / |\nabla \chi| \sim R / (B \delta r / a)$, one obtains

$$[(1/B) \nabla \chi \cdot \nabla \ln \mathcal{J}_{eq}]^2 \sim (\delta r / \delta r)^2 \sim 1. \quad (\text{B2})$$

Therefore, by using Eqs. (B1) and (B2), the first term on the right-hand side of Eq. (39) can be estimated as follows

$$\frac{g\mu_0 P' \kappa_n}{(\mathbf{B} \cdot \nabla \Lambda_s)^2} \sim (X_s^2 \mu_0 / B^2) \boldsymbol{\kappa} \cdot \nabla p. \quad (\text{B3})$$

The stability condition in Eq. (39) indicates that the right-hand side of Eq. (B3) should be larger than 1/4 for the instability to occur in the ideal MHD description.

-
- ¹ F. Wagner, G. Becker, K. Behringer, D. Campbell, A. Eberhagen, W. Engelhardt, G. Fussmann, O. Gehre, J. Gernhardt, G. V. Gierke, G. Haas, M. Huang, F. Karger, M. Keilhacker, O. Klüber, M. Kornherr, K. Lackner, G. Lisitano, G. G. Lister, H. M. Mayer, D. Meisel, E. R. Müller, H. Murmann, H. Niedermeyer, W. Poschenrieder, H. Rapp, H. Röhr, F. Schneider, G. Siller, E. Speth, A. Stäbler, K. H. Steuer, G. Venus, O. Vollmer, and Z. Yü, *Phys. Rev. Lett.* **49**, 1408 (1982). <https://doi.org/10.1103/PhysRevLett.49.1408>.
- ² P. B. Snyder, H. R. Wilson, J. R. Ferron, L. L. Lao, A. W. Leonard, T. H. Osborne, A. D. Turnbull, D. Mossessian, M. Murakami, and X. Q. Xu, Edge localized modes and the pedestal: A model based on coupled peeling–ballooning modes, *Phys. Plasmas* **9** 2037–2043 (2002). <https://doi.org/10.1063/1.1449463>.
- ³ C. M. Bishop, P. Kirby, J. W. Connor, R. J. Hastie, and J. B. Taylor, Ideal MHD ballooning stability in the vicinity of a separatrix, *Nucl. Fusion* **24** 1579 (1984). DOI 10.1088/0029-5515/24/12/006.
- ⁴ C. M. Bishop, Stability of localized MHD modes in divertor tokamaks – a picture of the H-mode, *Nucl. Fusion* **26** 1063 (1986). DOI 10.1088/0029-5515/26/8/006.
- ⁵ J. R. Myra, D. A. D'Ippolito, X. Q. Xu, R. H. Cohen, Resistive X-point modes in tokamak boundary plasmas *Phys. Plasmas* **7** 2290–2293 (2000). <https://doi.org/10.1063/1.874125>.
- ⁶ S. Saarelma, O. J. Kwon, A. Kirk, and the MAST Team, X-point effect on edge stability, *Plasma Phys. Control. Fusion* **53** 025011 (2011). doi:10.1088/0741-3335/53/2/025011.
- ⁷ A. J. Webster and C. G. Gimblett, Magnetohydrodynamic stability of a toroidal plasma's separatrix, *Physical Review Letters* **102**, 035003 (2009). DOI:<https://doi.org/10.1103/PhysRevLett.102.035003>.
- ⁸ A. J. Webster, Techniques for studying the separatrix of tokamak plasmas, *Physics of Plasmas* **16**, 012501 (2009). <https://doi.org/10.1063/1.3046070>.
- ⁹ L. C. Bernard, F. J. Helton, and R. W. Moore, GATO: An MHD stability code for axisymmetric plasmas with internal separatrices, *Comput. Phys. Commun.* **24**, 377-380 (1981). [https://doi.org/10.1016/0010-4655\(81\)90160-0](https://doi.org/10.1016/0010-4655(81)90160-0).
- ¹⁰ L. Degtyarev, A. Martynov, S. Medvedev, E. Troyon, L. Villard, and R. Gruber, The ideal MHD stability code for axisymmetric plasmas with separatrix, *Computer Physics Communications* **103**, 10-27 (1997). [https://doi.org/10.1016/S0010-4655\(97\)00037-4](https://doi.org/10.1016/S0010-4655(97)00037-4).
- ¹¹ A. D. Turnbull, J. M. Hanson, F. Turco, N. M. Ferraro, M. J. Lanctot, L. L. Lao, E. J. Strait, P. Piovesan, and P. Martin, The external kink mode in diverted tokamaks, *Journal of Plasma Physics* **82(3)** 515820301 (2016). doi:10.1017/S0022377816000568
- ¹² S. Yu Medvedev, A. A. Martynov, Y. R. Martin, O. Sauter, and L. Villard, Edge kink/ballooning mode stability in tokamaks with separatrix, *Plasma Physics and Controlled Fusion* **48**, 927 (2006). DOI 10.1088/0741-3335/48/7/003
- ¹³ Linjin Zheng, M. T. Kotschenreuther, and F. L. Waelbroeck, Asymptotic vacuum solution at tokamak X-point tip, *Phys. Plasmas* **30**, 112508 (2023). <https://doi.org/10.1063/5.0173656>
- ¹⁴ L. S. Solovév, The theory of hydrodynamic stability of toroidal plasma configurations *Sov. Phys. JETP* **26** 400 (1967). <http://www.jetp.ras.ru/cgi-bin/dn/e.026.02.0400.pdf>
- ¹⁵ A. Kirk, B. Koch, R. Scannell, H. R. Wilson, G. Counsell, J. Dowling, A. Herrmann, R. Martin, M. Walsh, and the MAST team, Evolution of Filament Structures during Edge-Localized Modes in the MAST Tokamak, *Phys. Rev. Lett.* **96**, 185001 (2006). DOI: 10.1103/PhysRevLett.96.185001.
- ¹⁶ F. Alladio, A. Mancuso and P. Micozzi, Rotating twisted filaments buoyancy: comparison between the convective region of the sun and the edge of a tokamak plasma, *Plasma Physics and Controlled Fusion* **50**, 124019 (2008). doi:10.1088/0741-3335/50/12/124019.
- ¹⁷ T. E. Evans, R. K. W. Roeder, J. A. Carter, and B. I. Rapoport, Homoclinic tangles, bifurcations and edge stochasticity in diverted tokamaks. *Contrib. Plasma Phys.* **44** 235-240 (2004). <https://doi.org/10.1002/ctpp.200410034>.
- ¹⁸ A. Kirk, J. Harrison, Yueqiang Liu, E. Nardon, T. Chapman, P. Denner, and the MAST team, Observation of Lobes near the X Point in Resonant Magnetic Perturbation Experiments on MAST, *Phys. Rev. Lett.* **108** 255003 (2012). DOI: 10.1103/PhysRevLett.108.255003.
- ¹⁹ A. Kirk, I.T. Chapman, Yueqiang Liu, P. Cahyna, P. Denner, G. Fishpool, C.J. Ham, J.R. Harrison, Yunfeng

- Liang, E. Nardon, S. Saarelma, R. Scannell, A.J. Thornton, and the MAST Team, Understanding edge-localized mode mitigation by resonant magnetic perturbations on MAST, *Nucl. Fusion* **53** 043007 (2013). DOI 10.1088/0029-5515/53/4/043007.
- ²⁰ R. C. Grimm, J. M. Greene, J. L. and Johnson, *Methods of Computational Physics* (Academic, New York, 1976).
- ²¹ G. Bateman and Y.-K. M. Peng, Magnetohydrodynamic Stability of Flux-Conserving Tokamak Equilibria, *Phys. Rev. Lett.* **15** 829 (1977). DOI:<https://doi.org/10.1103/PhysRevLett.38.829>.
- ²² C. Mercier, Critere de stabilite d'an systeme toroidal hydromagnetique en pression scalaire *Nucl. Fusion Suppl.* **2** 801 (1962).
- ²³ J. M. Greene and J. L. Johnson, Stability criterion for arbitrary hydromagnetic equilibria, *Phys. Fluids* **5** 510-17 (1962). <https://doi.org/10.1063/1.1706651>.
- ²⁴ A. H. Glasser, The direct criterion of Newcomb for the ideal MHD stability of an axisymmetric toroidal plasma, *Phys. Plasmas* **23** 072505 (2016). <https://doi.org/10.1063/1.4958328>
- ²⁵ L. J. Zheng, M. T. Kotschenreuther, and P. Valanju, The sensitivity of tokamak magnetohydrodynamics stability on the edge equilibrium, *Phys. Plasmas* **24** 102503 (2017). <https://doi.org/10.1063/1.4986036>
- ²⁶ L.-J. Zheng and M. Kotschenreuther, AEGIS: An adaptive ideal-magnetohydrodynamics shooting code for axisymmetric plasma stability, *J. Comput. Phys.* **211** 748 (2006). <https://doi.org/10.1016/j.jcp.2005.06.009>.
- ²⁷ John M. Greene and John L. Johnson, Interchange instabilities in ideal hydromagnetic theory, *Plasma Phys.* **10** 729 (1968). DOI 10.1088/0032-1028/10/8/301.
- ²⁸ D. Lortz, The general "peeling" instability, *Nucl. Fusion* **15** 49 (1975). DOI 10.1088/0029-5515/15/1/007.
- ²⁹ J. Hastie, private communication, published in J. A. Wesson, Hydromagnetic stability of tokamaks, *Nuclear Fusion* **18** 87 (1978). DOI 10.1088/0029-5515/18/1/010.
- ³⁰ A. H. Glasser, J. M. Greene, and J. L. Johnson, Resistive instabilities in general toroidal plasma configurations, *Phys. Fluids* **18**, 875-888 (1975). <https://doi.org/10.1063/1.861224>.
- ³¹ Linjin Zheng, *Magnetically confined fusion plasma physics: ideal MHD theory* (Morgan & Claypool Publishers, San Rafael, California and IOP Publishing, Bristol, UK 2019). DOI 10.1088/978-1-64327-138-5.
- ³² A. H. Glasser, J. M. Greene, and J. L. Johnson, Resistive instabilities in a tokamak *Phys. Fluids* **19**, 567 (1976). <https://doi.org/10.1063/1.861490>.
- ³³ J. W. Connor, R. J. Hastie, and J. B. Taylor, High mode number stability of an axisymmetric toroidal plasma, *Proc. R. Soc. A* **365**, 1 (1979). <https://doi.org/10.1098/rspa.1979.0001>.
- ³⁴ H. L. Berk, M. N. Rosenbluth, and J. L. Shohet, Ballooning mode calculations in stellarators, *Phys. Fluids* **26** 2616 (1983). <https://doi.org/10.1063/1.864453>.
- ³⁵ A. Yolbarsop, F. Porcelli, and R. Fitzpatrick, Impact of magnetic X-points on the vertical stability of tokamak plasmas, *Nuclear Fusion* **61**,114003 (2021). <https://doi.org/10.1088/1741-4326/ac27c5>.
- ³⁶ A. Yolbarsop, F. Porcelli, W. Liu and R. Fitzpatrick, Analytic theory of ideal-MHD vertical displacements in tokamak plasmas, *Plasma Physics and Controlled Fusion* **64**, 105002 (2022). <https://doi.org/10.1088/1361-6587/ac7ee6>.
- ³⁷ T. Barberis, A. Yolbarsop, and F. Porcelli, Vertical displacement oscillatory modes in tokamak plasmas, *Journal of Plasma Physics* **88**, 905880511 (2022). <https://doi.org/10.1017/S0022377822000988>.
- ³⁸ W. M. Tang, J. W. Connor, and R. J. Hastie, Kinetic-ballooning-mode theory in general geometry, *Nucl. Fusion* **20** 1439 (1980). DOI 10.1088/0029-5515/20/11/011.
- ³⁹ L. J. Zheng, M. T. Kotschenreuther, and J. W. Van Dam, Revisiting linear gyrokinetics to recover ideal magnetohydrodynamics and missing finite Larmor radius effects, *Phys. Plasmas* **14** 072505 (2007). <https://doi.org/10.1063/1.2746811>
- ⁴⁰ B. Hudson, T. Evans, C. Petty, and P. Snyder, Dependence of resonant magnetic perturbation experiments on the DIII-D plasma shape, *Nucl. Fusion* **50**, 064005 (2010). DOI: [doi:10.1088/0029-5515/50/6/064005](https://doi.org/10.1088/0029-5515/50/6/064005).